Journal of Materials Chemistry A

Accepted Manuscript

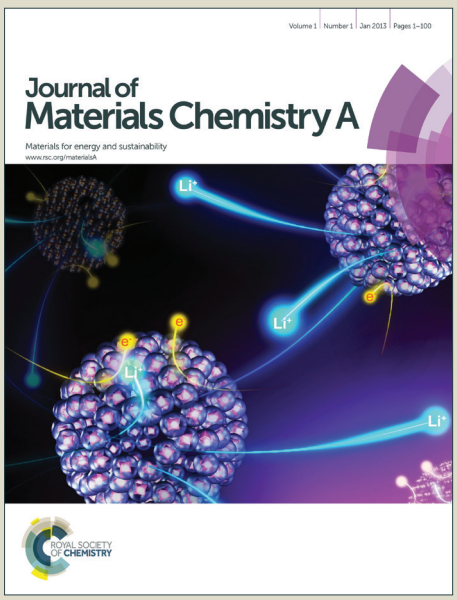

This is an *Accepted Manuscript*, which has been through the Royal Society of Chemistry peer review process and has been accepted for publication.

Accepted Manuscripts are published online shortly after acceptance, before technical editing, formatting and proof reading. Using this free service, authors can make their results available to the community, in citable form, before we publish the edited article. We will replace this *Accepted Manuscript* with the edited and formatted *Advance Article* as soon as it is available.

You can find more information about *Accepted Manuscripts* in the Information for Authors.

Please note that technical editing may introduce minor changes to the text and/or graphics, which may alter content. The journal's standard Terms & Conditions and the Ethical guidelines still apply. In no event shall the Royal Society of Chemistry be held responsible for any errors or omissions in this *Accepted Manuscript* or any consequences arising from the use of any information it contains.

ROYAL SOCIETY OF CHEMISTRY

www.rsc.org/materialsA

Journal of Materials Chemistry A RSCPublishing

ARTICLE

Three-dimensional $Au_{0.5}$/RGO/$Au_{0.5}$/RGO/CF electrode and its high catalytic performances toward ethanol electrooxidation in alkaline medium

Cite this: DOI: 10.1039/xoxxoooooox

Received ooth January 2012,
Accepted ooth January 2012

DOI: 10.1039/xoxxoooooox

www.rsc.org/

Caiqin Wang,[a] Huiwen Wang,[a] Chunyang Zhai,[a] Fangfang Ren,[a] Mingshan Zhu,*[b] Ping Yang[a] and Yukou Du*[a]

A three-dimensional Au nanoparticles/graphene/carbon fibers hybrid electrode was fabricated by a layer-by-layer method, denoted as $Au_{0.5}$/RGO/$Au_{0.5}$/RGO/CF. The as-formed composite was characterized by Raman spectroscopy, X-ray diffraction (XRD), scanning electron microscope (SEM) and X-ray photoelectron spectroscopy (XPS). It was found that two layers of reduced graphene oxide (RGO) sheets and two layers of Au nanoparticles were assembled alternately on carbon fibers. The catalytic performances of as-prepared electrode were evaluated via the cyclic voltammetry (CV) and chronopotentiometry (CA) measurements. It was demonstrated that the as-synthesized 3D $Au_{0.5}$/RGO/$Au_{0.5}$/RGO/CF electrode exhibited highly efficient electrocatalytic activity toward ethanol oxidation in alkaline medium and Au NPs was not affected by the covered graphene layers. The synergetic interaction between RGO sheets and Au nanoparticles enhanced the catalytic activity of the electrode. Meanwhile, the excellent electron conductivity of RGO sheets benefited to the electron transfer and the oxidation removal of the intermediate species during the ethanol electrooxidation, which was good to the catalytic activity. Because of the effects of the above multiple factors, the $Au_{0.5}$/RGO/$Au_{0.5}$/RGO/CF electrode exhibited well catalytic performances.

1. Introduction

Due to the shortage of future energy source, the concerns about the search for alternative energy sources have increasingly appealed to the worldwide scientists' attention in the last decades. Directed ethanol fuel cells (DEFCs) can be considered as one of the most promising technologies because of less toxic, higher energy densities, easy storability and refueling of ethanol fuels.[1-3] Traditionally, platinum and platinum-based materials have been extensively studied as active catalysts for ethanol electrooxidation in DEFCs.[3-5] However, the large-scale commercialization of DEFCs has been hindered by the sluggish reaction dynamics, the high cost and limited supply of platinum. In recent few decades, a number of studies have focused on non-platinum electrocatalysts.[6-9]

Au is one of the interesting candidates. Traditionally, Au is once considered to be chemically inert. But recent studies show that Au nanoparticles exhibit high catalytic activity.[10-13] Au in nanoscale has exhibited a series of fascinating aspects such as their assembly of multiple types involving materials science, the behavior of the individual particles, size-related electronic, magnetic and optical properties (quantum size effect).[12,13] Compared with Pt, Au is not prone to get poisoned by CO.[10] And Au nanoparticles could exhibit unusual activity and selectivity in a wide array of reactions, such as the CO oxidation, water gas shift reaction and alcohols electrooxidation.[13-18] Based on these fascinating properties, Au maybe be an interesting candidate to replace Pt in somehow. More recently, the electrooxidation of ethanol on gold nanoparticles has been the focus of many research studies.[13,18] Typically, Koper et al.[3] have applied gold as a model electrocatalyst to study the pathway of ethanol oxidation. They further deduced that the ethanol oxidation reaction on gold in alkaline media is mainly via C_2-pathway (oxidation of ethanol to acetaldehyde and ultimately to acetic acid/acetate) but not the C_1 pathways with the carbon–carbon bond break. Also they investigated the effect of electrolyte pH on the ethanol oxidation reaction on gold, concluding that ethanol oxidation does not take place on Au at an appreciable rate when pH value is less than 6. And as pH value is higher than 6, the oxidation of ethanol on Au apparently increased with pH value. Rodriguez and Koper[19] also indicated that the electrocatalysis of redox reactions on gold is highly pH dependent, often preferring alkaline media. They pointed out that the high activity of gold for the oxidation of alcohols in alkaline media is related to the favorable reaction conditions in solution combined with the low tendency of gold that was poisoned by either CO or surface

Journal of Materials Chemistry A Accepted Manuscript

oxides, due to the fact that gold does not bind the neutral intermediates strongly enough.

DFT studies suggest that the high catalytic activity of Au nanoparticles is associated with the presence of atoms with very low coordination number, and the supporting material also seems to play important role in the process.[20,21] Metal oxides such as TiO_2, CeO_2, ZnO and Mn_3O_4, are a species of traditional supporting materials which are widely used in catalytic field.[21-24] For example, Holz et al.[23] and Sobolev et al.[24] investigated the gas-phase oxidation of ethanol over the Au/TiO_2 catalyst. In Idriss's report, the reaction of ethanol has been investigated on the surface of Au/CeO_2.[25] It is generally agreed that the combination of Au-NPs on certain metal oxide supports should be responsible for the enhanced activity.[16]

Graphene, as a novel supporting material with the sp^2-bonded carbon atoms arraying hexagonally, has been extensively studied in physics, chemistry and materials fields due to its excellent properties such as large surface area (~2600 m^2 g^{-1}), high electrical conductivity (105-106 S m^{-1}), rapid heterogeneous electron transfer and outstanding mechanical properties.[26-29] Inspired by its novel properties, graphene is widely used to improve the activity of metal nanoparticles in recent years. And a lot of noble metal nanoparticles/graphene composites have been synthesized.[30-33] Zhu et al.[34] fabricated graphene–Au NPs hybrid films and studied its high-performance surface-enhanced Raman scattering substrates for detecting organic molecules such as rhodamine-6G. Huang et al.[35] synthesized the Au–RGO nanocomposite using UV irradiation assisting Au–reduced graphene oxide, and its electrochemical sensing performance toward TNT had been investigated. In our previous work[36], the N-Pt/RGO/CF electrode was synthesized via a layer-by-layer method and used for the electro-oxidation of methanol. The N-Pt/RGO/CF electrode showed good electrochemical properties and enhanced electrocatalytic activity toward methanol electrooxidation. Besides the excellent properties of graphene, the functional groups on the graphene oxide precursor could provide favorable sites for anchoring the effective metal catalyst components as well as adsorbing the reaction species, resulting more interaction states, transmission channels generated between them.[37-39] These collective factors ultimately promote the catalytic performances of catalyst.

In this work, we fabricated the three-dimensional (3D) Au nanoparticles/graphene/carbon fibers hybrid electrode and used it for ethanol electrooxidation in alkaline medium. The aim of the present study is to elucidate the influence of the introduction of graphene sheets covered on the Au nanoparticles layers on the electrocatalytical oxidation of ethanol. The following questions have been addressed in this work: Can the effective 3D electrode be constructed by the simple layer-by-layer method? What is the role of graphene in the 3D electrode? Covered by layers of graphene, if the activity of the Au nanoparticles toward ethanol electrooxidation will be inhibited? Are there synergetic effects between Au nanoparticles and graphene? Can the particular structure enhance the catalytic activity towards ethanol oxidation? To answer the questions, a series of electrodes have been designed, fabricated and characterized.

2. Experimental section

2.1. Materials and apparatus

Carbon fibers (CF, length 15mm) were purchased from the commercial carbon cloth company (WOS 1002 CeTech CO., Ltd., China). $HAuCl_4$ (Shanghai shiyi Chemicals reagent Co., Ltd., China) was used as precursors for the preparation of Au nanoparticles. C_2H_5OH, H_3PO_4, and KOH were all of analytical grade and used without further purification. Doubly distilled water was used throughout the experiments. Na-PBS (Na_2HPO_4/NaH_2PO_4, 0.01 M, pH = 4.2) was prepared to use as electrolyte in the electrochemical reduction of graphene. The electrolytes of 1.0 M KOH and 1.0 M C_2H_5OH/1.0 M KOH solution were prepared previously for use in the electrochemical experiments.

All electrochemical experiments were performed in a conventional three–electrode–cell system at room temperature on a CHI 760E potentiostat/galvanostat (CH Instrumental Co., Ltd., China). The CF and modified CF were fixed onto the electrical wires to use as working electrodes. Platinum wire was used as counter electrode and the saturated calomel electrode (SCE) was used as reference electrode. The electrochemical measurements such as cyclic voltammetry (CV), chronoamperometry (CA), and electrochemical impedance spectroscopy (EIS) were performed in 1.0 M KOH and/or 1.0 M CH_3OH/1.0 M KOH solution. The EIS was recorded between 0.1 Hz and 10^5 Hz with the AC voltage amplitude 5.0 mV. All potentials reported in this paper have been converted to RHE scale. The solutions were deaerated by purging with dry nitrogen stream, and a slight nitrogen overpressure was kept during electrochemical experiments.

2.2. Preparation of $Au_{0.5}$/RGO/$Au_{0.5}$/RGO/CF electrodes

The schematic representation of preparation processes of the electrodes was shown in Scheme 1. Specifically, for $Au_{0.5}/RGO/Au_{0.5}/RGO/CF$, 10 μL graphene oxide (GO) aquaous solution (0.5 mg mL^{-1}) that was prepared by a modified Hummers' method,[36,40] was dripped onto the CF electrodes and dried in an oven at 70 °C. Then the GO on the surface of CF electrode was electrochemically reduced into reduced graphene oxide (RGO) by a potentiostatic method at 0.15 V (*vs*. RHE) for 1000 s in Na-PBS solution. The RGO sheets were considered as the first layer of the $Au_{0.5}/RGO/Au_{0.5}/RGO/CF$ electrode. After that, Au nanoparticles were electrodeposited onto the RGO modified CF electrode in 3 mM $HAuCl_4$/0.5 M H_3PO_4 solution at a constant potential of 0.85 V with electrodeposition charge of 2.5×10^{-3} C. This was the second layer of the electrode. Subsequently and similarly, another 10 μL graphene oxide (GO) aquaous solution was dripped onto the modified electrode and electrochemically reduced to obtain RGO sheets, which constructed the third layer of the $Au_{0.5}/RGO/Au_{0.5}/RGO/CF$ electrode. Finally, Au nanoparticles were electrodeposited again with electrodeposition charge of 2.5×10^{-3} C via the same method as before, which constructed the forth layer of the modified electrode. Then the as-obtained $Au_{0.5}/RGO/Au_{0.5}/RGO/CF$ was rinsed with doubly distilled water for use in the following.

For Au/RGO/CF, 20 μL GO solution were dripped onto the CF electrode by drop. After it was dried, the GO on the modified electrode was electrochemically reduced as similarly as before. Then Au particles were electrodeposited by the same method in 3 mM $HAuCl_4$/0.5 M H_3PO_4 solution with charge of 5.0×10^{-3} C. And for Au/CF, Au particles were directly electrodeposited onto the bare CF electrode with electrodepositing charge of 5.0×10^{-3} C.

For the comparative electrodes, such as $Au_{0.25}/RGO/Au_{0.75}/RGO/CF$ and $Au_{0.75}/RGO/Au_{0.25}/RGO/CF$,

Journal of Materials Chemistry A Accepted Manuscript

This journal is © The Royal Society of Chemistry 2012

the overall amounts of loading Au particles and/or RGO were kept in correspondence with the $Au_{0.5}$/RGO/$Au_{0.5}$/RGO/CF electrode. Based on the integrated charge of gold electro-deposition and assumed a 100% current efficiency, the overall amount of loading Au was estimated to about 3.4 μg according to the Faraday's Law.

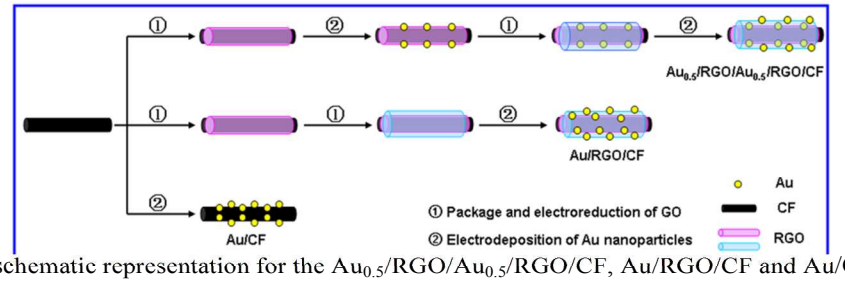

Scheme 1 A schematic representation for the $Au_{0.5}$/RGO/$Au_{0.5}$/RGO/CF, Au/RGO/CF and Au/CF electrodes.

2.3. Characterization

Scanning electron microscope (SEM, S–4700, Japan) was performed to obtain the morphology of samples. Raman spectra were collected on a micro–Raman spectroscopy (LabRam HR800) system equipped with 514.5 nm laser. X-ray diffraction (XRD) analysis was carried out on PANalytical X'Pert PRO MRD X-ray diffractometer (PANalytical Company, Holland) with Cu Ka radiation (λ=1.54056 Å) operated at 40 kV and 30 mA. X-ray photoelectron spectroscopy (XPS) was obtained on an ESCALab220i-XL electron spectrometer from VG Scientific with 300 W Al Kα X-ray radiation as the X-ray source for excitation.

Inductively coupled plasma emission spectrometer (ICP, Vista MPX, Varian Medical Systems, USA) was investigated to determine the actual Au loadings after digestion of samples in a 3:1 HCl/HNO_3 mixture. The results were shown in Table 1. As seen, the values obtained by ICP are rather closed to that calculated according to the electrodepositing charge. Given that the total electrodepositing charges of Au on the comparative electrodes are the same, and in order to make the comparative basis uniform among the electrodes, the Au amounts in the whole manuscript were unified with the calculated value via the electrodepositing charge according to the Faraday's Law.

Table 1 Summarized amount of Au determined by ICP analysis and amount of Au calculated using the electrodepositing charge on different electrodes.

Electrodes	The amount of Au determined by ICP/ μg	The calculated amount of Au according to the electrodepositing charge/ μg
$Au_{0.5}$/RGO/$Au_{0.5}$/RGO/CF	3.33	3.40
Au/RGO/CF	3.36	3.40
Au/CF	3.34	3.40

3. Results and discussion

3.1. Morphological and structural characterization of electrodes

Typical SEM images of bare CF and RGO/CF electrodes are shown in Fig. 1A and B, respectively. As is observed from Fig. 1A, the tiny carbon fiber exhibits smooth surface with a diameter of about 10 μm. After coated with RGO (Fig.1B), it can be seen that the surface of CF was wrapped by the wrinkled RGO sheets. The RGO sheets with wrinkles would supply more active sites for nuclei and growth of the following Au deposition and/or the adsorption of reaction species.

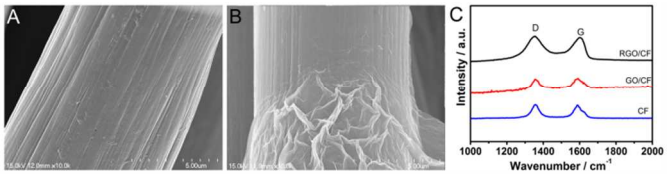

Fig. 1 SEM images of bare CF (A) and RGO modified CF (B); and (C) Raman spectra of bare CF, GO/CF and RGO/CF nanostructures.

Raman spectroscopy can give some important analytical information about the characteristics of the inner structure (e.g. defects) of the carbonaceous materials.[41-43] The Raman spectra of bare CF, GO/CF and RGO/CF are presented in Fig. 1C. As seen, all samples display a similar Raman spectrum in terms of the shapes and positions of the Raman peaks. The appearance of two prominent peaks at around 1351 cm^{-1} and 1597 cm^{-1} are ascribed to the D and G bands of carbon materials, respectively.[30,36] The D band is associated with the out-of-plane vibrational modes and the disordered structural defects or edge areas, and the G band is related to the in-plane vibration of sp^2 bonded carbon atoms.[44] In addition, the intensity ratio of the D and G bands (I_D/I_G) can provide extraordinary information because it is proportional to the average size of sp^2 domains and the structural disorder of graphene sheets. As estimated, the I_D/I_G of bare CF is about 1.08. After coated with GO, the I_D/I_G of GO/CF was reduced to 0.98, indicating the decrease of disordering degree because of the presence of defects in GO. As GO was electrochemically reduced into RGO, the I_D/I_G ratio increased from 0.98 (on GO/CF) to 1.02 (on RGO/CF), which implied the reduction in the plane sp^2 domains, or the realization of deoxygenation during the reduction of GO.[30,45]

Fig. 2(A-C) shows the SEM images of $Au_{0.5}$/RGO/CF, RGO/$Au_{0.5}$/RGO/CF and $Au_{0.5}$/RGO/$Au_{0.5}$/RGO/CF that was prepared by a layer-by-layer method, respectively. From these images, the mophorlogy of $Au_{0.5}$/RGO/$Au_{0.5}$/RGO/CF electrode during fabrication can be clearly observed. After RGO sheets covered the CF electrode as the first layer of the modified electrode (Fig. 1B), the Au particles were electrodeposited onto the RGO modified CF as the second layer, shown in Fig. 2A. It can be seen that the Au nanoparticles with sharp tips were dispersed well on the RGO sheets modified CF. Then the other layer of RGO sheets was coated onto the modified electrode, shown in Fig. 2B. The Au particles could be observed through the gauze-like RGO sheets. Finally, the Au particles were again elecrodeposited onto the modified CF electrode with the same electrodepositing charge as before. As can be seen in Fig. 2C, the outer-layer Au nanoparticles uniformly disperse on the surface of modified electrode and present the needle-like structure with sharp tips. And it is worth noticing that

Journal of Materials Chemistry A Accepted Manuscript

the inner-layer Au particles could be distinguished as well through the coating RGO layers (Fig. 2C). These results indicate that the as-prepared $Au_{0.5}$/RGO/$Au_{0.5}$/RGO/CF electrode exhibits particular three-dimensional (3D) structure.

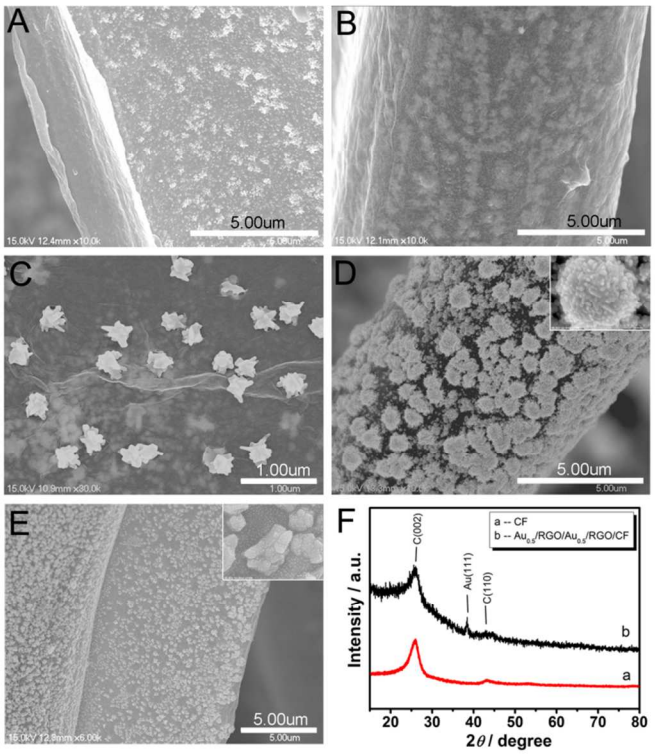

Fig. 2 SEM images of $Au_{0.5}$/RGO/CF (A), RGO/$Au_{0.5}$/RGO/CF (B), $Au_{0.5}$/RGO/$Au_{0.5}$/RGO/CF (C), Au/CF (D), and Au/RGO/CF (E); and (F) XRD patterns of bare CF and $Au_{0.5}$/RGO/$Au_{0.5}$/RGO/CF.

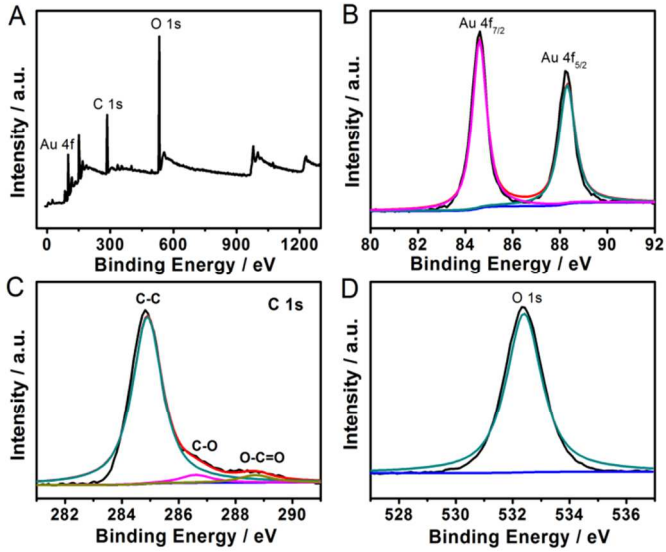

Fig. 3 XPS spectra of $Au_{0.5}$/RGO/$Au_{0.5}$/RGO. (A) Survey scan of the spectral region from 0 to 1300 eV; (B) Au 4f region; (C) C 1s region; and (D) O 1s region. The spectra were obtained by calibration based on C 1s peak at 284.5 eV.

Fig. 2D and E display the SEM images of the comparative electrodes, Au/CF and Au/RGO/CF, respectively. For Au/CF, as seen in Fig. 2D, Au nanoparticles accumulate obviously on bare CF. While on the surface of Au/RGO/CF (Fig. 2E), the Au nanoparticles dispersed better compared with that on Au/CF. This may be due to the fact that the RGO sheets with wrinkles increase the surface area of electrode and supply more active sites, which are beneficial to the deposition of Au nanoparticles.

XRD analysis was performed to further study the structure of the $Au_{0.5}$/RGO/$Au_{0.5}$/RGO/CF electrode (Fig. 2F). The diffraction peaks located at the 2θ values of 26° and 42° on both bare CF and $Au_{0.5}$/RGO/$Au_{0.5}$/RGO/CF are assigned to the C(002) and C(110), respectively. The 2θ peak at around 38.5° on $Au_{0.5}$/RGO/$Au_{0.5}$/RGO/CF is attributed to the diffraction of Au (111). And the average size of the Au nanoparticles was calculated from the half-width of the Au (111) diffraction peak using the Debye–Scherrer equation,[44,46,47] which was estimated to be about 17.6 nm.

The XPS analysis has been performed on $Au_{0.5}$/RGO/$Au_{0.5}$/RGO to obtain information about the oxidation state of Au nanoparticles and their interaction with RGO sheets. The XPS spectra of $Au_{0.5}$/RGO/$Au_{0.5}$/RGO (Fig. 3A) show the presence of Au 4f, C 1s, and O 1s peaks. Fig. 3B displays the Au 4f spectrum of Au nanoparticles loaded on RGO sheets. The spectra could be resolved to two typical well-separated doublets at 84.6 and 88.3 eV binding energy (BE), which is assigned to the binding energy of Au $4f_{7/2}$ and Au $4f_{5/2}$ in zero-valent state, respectively.[48,49] According to the reports in literatures,[50,51] the Au^0 peaks were shifted toward a higher BE with respect to the BE for bulk Au (83.9 and 87.4 eV), attributed to the Au bonded to O remaining in the reduced GO. The C 1s XPS spectrum for Au/RGO/Au/RGO is presented in Fig. 3C. The C 1s peaks can be fitted into three different components of oxygen-containing functional groups: (a) non-oxygenated C at 284.8 eV, corresponding to the graphite-like sp^2 hybridized carbon (C–C); (b) epoxy carbon (C–O) at 286.8 eV; and (c) carbonyl carbon (O–C=O) at 288.7eV.[31,48,49] As shown in Fig. 3D, the O 1s binding energy is located at 532.4 eV, which is assigned to the chemisorbed oxygen species (O^{2-}) remaining in reduced GO sheets.[52]

3.2. The catalytic performances of as-prepared electrodes

Fig. 4A presents the CVs of $Au_{0.5}$/RGO/$Au_{0.5}$/RGO/CF, Au/RGO/CF and Au/CF electrodes in 1.0 M KOH aqueous solution. The CVs of these electrodes do not present obvious hydrogen adsorption/desorption peaks during the scan in the range between 0.55 and 0.8 V. And there is an oxidation peak between 0.9 and 1.2 V in the forward scan, which is probably attributed to the formation of gold oxides on the gold surface.[53] In the reverse scan, this oxide film was reduced, releasing the active sites on Au surface.[54,55] The current consumed to reduce the surface oxide in the peak can be used to determine the electrochemically active surface area (ECSA, cm^2 mg^{-1}_{Au}) of Au according to the equation ECSA = Q/0.386×[Au],[54-56] where Q (mC) is the total charge for the reduction of AuO; 0.386 (mC cm^{-2}) is a constant assuming that a monolayer of AuO was formed on Au surface; and [Au] is the mass of loading Au on electrode. The ECSA was estimated to be 2.1, 0.8, 0.7 cm^2 mg^{-1}_{Au} for $Au_{0.5}$/RGO/$Au_{0.5}$/RGO/CF, Au/RGO/CF and Au/CF, respectively. The large ECSA indicated that the $Au_{0.5}$/RGO/$Au_{0.5}$/RGO/CF has a higher number of available metallic surfaces to reaction takes place, in other words, even more sites, which can be used by the reaction. On the other hand, it is apparently in Fig. 4A that the background current of $Au_{0.5}$/RGO/$Au_{0.5}$/RGO/CF

Journal of Materials Chemistry A Accepted Manuscript

This journal is © The Royal Society of Chemistry 2012

is the highest, suggesting the greatest capacitive behaviour on $Au_{0.5}$/RGO/$Au_{0.5}$/RGO/CF compared with that on both Au/RGO/CF and Au/CF electrodes.[57] Also it implies that the $Au_{0.5}$/RGO/$Au_{0.5}$/RGO/CF electrode has the relatively large surface area.[58]

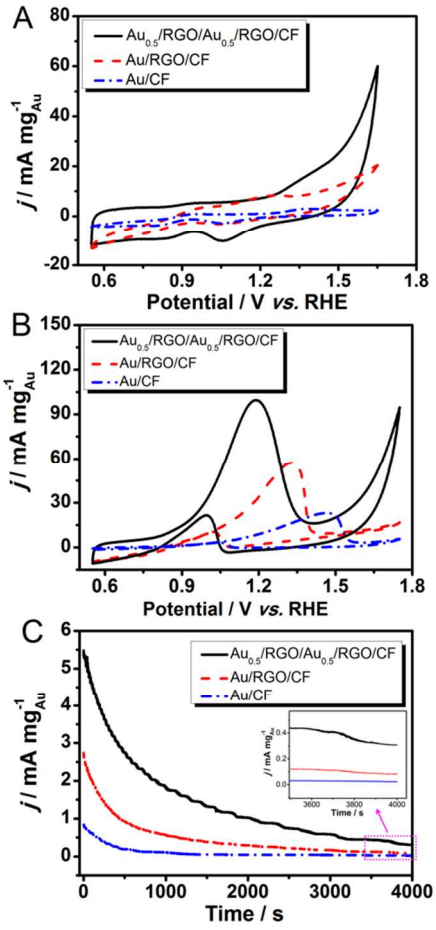

Fig. 4 (A) Cyclic voltammograms (CVs) of $Au_{0.5}$/RGO/$Au_{0.5}$/RGO/CF, Au/RGO/CF and Au/CF in 1.0 M KOH solution at a scan rate of 50 mV s^{-1}, respectively; (B) cyclic voltammograms (CVs) and (C) chronoamperograms (CAs) of $Au_{0.5}$/RGO/$Au_{0.5}$/RGO/CF, Au/RGO/CF and Au/CF at 0.65 V (*vs.* RHE) in 1.0 M C_2H_5OH/1.0 M KOH solution. The inset in Fig. 4C is the partial magnification pattern of CAs.

The catalytic activity of $Au_{0.5}$/RGO/$Au_{0.5}$/RGO/CF, Au/RGO/CF and Au/CF electrodes toward ethanol electrooxidation was measured by cyclic voltammetry (CV) in 1.0 M C_2H_5OH/1.0 M KOH solution, shown in Fig. 4B. As to keep the comparative basis to be uniformed, the specific activities of ethanol electro-oxidation in all electrochemical experiments were represented according to the current densities, which were normalized by per milligram of Au ladings calculated via the electrodepositing charge. As seen, the peaks in the forward scan are ascribed to the oxidation of freshly chemisorbed species resulting from ethanol adsorption.[59] The peak current density on $Au_{0.5}$/RGO/$Au_{0.5}$/RGO/CF electrode was 100.5 mA mg^{-1}_{Au}, which was about 1.7 and 4 times higher than that on Au/RGO/CF (58.7 mA mg^{-1}_{Au}) and Au/CF (24.6 mA mg^{-1}_{Au}), respectively. Additionally, we calculated the surface area normalized current density (mA cm^{-2}) based on electrochemical active surface area of Au, which are 47.6, 73.4 and 35.1 mA cm^{-2} for $Au_{0.5}$/RGO/$Au_{0.5}$/RGO/CF, Au/RGO/CF and Au/CF, respectively. It should be noted that the ECSA normalized peak current density of $Au_{0.5}$/RGO/$Au_{0.5}$/RGO/CF is lower than that of Au/RGO/CF electrode. Meanwhile, compared with the reported results, the ECSA normalized peak current density of $Au_{0.5}$/RGO/$Au_{0.5}$/RGO/CF electrode (47.6 mA cm^{-2}) is higher than that of some similar materials.[56,60] For example, it is over 14 times as high as the Au-PANI nanocomposite modified electrode (3.36 mA cm^{-2}) reported in Pandey's work,[60] and nearly 4 times as high as the Au NFs/CFC electrode (about 12 mA cm^{-2}) prepared by Yang.[56] Besides, it can be seen that the potential of oxidation peak on $Au_{0.5}$/RGO/$Au_{0.5}$/RGO/CF (1.18 V) is more negative than that on Au/RGO/CF (1.33 V) and Au/CF (1.48 V). The notably large peak current density and the relatively negative peak potential indicated that the $Au_{0.5}$/RGO/$Au_{0.5}$/RGO/CF electrode has good catalytic activity and enhanced kinetics toward ethanol electrooxidation reaction.[61]

The long-time stability of $Au_{0.5}$/RGO/$Au_{0.5}$/RGO/CF, Au/RGO/CF and Au/CF electrodes toward ethanol electrooxidation was also measured via the chronoamperometry (CA) measurement in 1.0 M C_2H_5OH/1.0 M KOH solution. The chronoamperograms (CAs) were carried out at 0.65 V (*vs.* RHE), recorded in Fig. 4C. As seen, the current densities at initial stage on these three electrodes were low, which is possibly due to the low oxidation kinetics at the applied potential. Despite this, the current density on $Au_{0.5}$/RGO/$Au_{0.5}$/RGO/CF is higher than that on the other two electrodes, which indicated that the relatively high reaction kinetics on $Au_{0.5}$/RGO/$Au_{0.5}$/RGO/CF. Subsequently, the current densities on all electrodes undergo an inevitable decrease at the initial stage. This is probably due to the unavoidable formation of Au-oxides and/or the decrease of active sites that were occupied by reaction intermediates (e.g. alkoxide and acetaldehyde species) generated during ethanol electrooxidation. Then the current densities tend to be steady gradually. After scanning for 4000 s, as seen clearly in the inset, the final current density on $Au_{0.5}$/RGO/$Au_{0.5}$/RGO/CF is still the highest in comparison with that on Au/RGO/CF and Au/CF electrodes. This suggests that $Au_{0.5}$/RGO/$Au_{0.5}$/RGO/CF electrode possesses the great stability toward ethanol oxidation. The above CV and CA results demonstrate that the $Au_{0.5}$/RGO/$Au_{0.5}$/RGO/CF electrode has better catalytic performances than Au/RGO/CF and Au/CF electrodes. It is probably attributed to the particular 3D structure of $Au_{0.5}$/RGO/$Au_{0.5}$/RGO/CF. The alternately assembled RGO layers and Au nanoparticles layers on $Au_{0.5}$/RGO/$Au_{0.5}$/RGO/CF boosted more interaction states, transmission channels as well as nanoscale junctions between Au nanoparticles and RGO sheets compared with Au/RGO/CF and Au/CF electrodes, which promoted the catalytic properties of electrode.

3.3. The effects of the distributions of Au nanoparticles and RGO sheets on catalytic performances for ethanol oxidation

In order to investigate how the different distribution of Au nanoparticles in the 3D electrodes effects on their catalytic activities, a series of electrodes were prepared, including $Au_{0.25}$/RGO/$Au_{0.75}$/RGO/CF, $Au_{0.5}$/RGO/$Au_{0.5}$/RGO/CF, and $Au_{0.75}$/RGO/$Au_{0.25}$/RGO/CF. The total Au electrodeposition charges of these three electrodes were fixed to be 5×10^{-3} C. And their catalytic performances toward ethanol electrooxidation were evaluated by cyclic voltammetry and chronoamperometry measurements, respectively. Fig. 5A records the cyclic voltammograms (CVs) of these electrodes in 1.0 M KOH solution containing 1.0 M C_2H_5OH. As seen, the peak current densities on the

Journal of Materials Chemistry A Accepted Manuscript

Au/RGO/Au/RGO/CF electrodes are almost equal, which is possibly due to the same amount of total Au loadings on the Au/RGO/Au/RGO/CF electrodes. While there are obvious shifts among the oxidation peak potentials, which increase in the following order: $Au_{0.5}$/RGO/$Au_{0.5}$/RGO/CF (1.18 V) < $Au_{0.75}$/RGO/$Au_{0.25}$/RGO/CF (1.46 V) < $Au_{0.25}$/RGO/$Au_{0.75}$/RGO/CF (1.57 V). The relatively negative oxidation peak potential on $Au_{0.5}$/RGO/$Au_{0.5}$/RGO/CF suggests that it has low overpotential, which is owing to its low mass-transfer resistance.[62, 63] Meanwhile, it can be seen that the onset oxidation potential (E_{onset}) on $Au_{0.5}$/RGO/$Au_{0.5}$/RGO/CF is 0.75 V, which is lower than that on $Au_{0.75}$/RGO/$Au_{0.25}$/RGO/CF (0.84 V) and $Au_{0.25}$/RGO/$Au_{0.75}$/RGO/CF (0.89 V). The lower E_{onset} indicates that the $Au_{0.5}$/RGO/$Au_{0.5}$/RGO/CF electrode has better catalytic activity toward ethanol electrooxidation in comparison with $Au_{0.75}$/RGO/$Au_{0.25}$/RGO/CF and $Au_{0.25}$/RGO/$Au_{0.75}$/RGO/CF. The low oxidation peak potential and E_{onset} on $Au_{0.5}$/RGO/$Au_{0.5}$/RGO/CF are possibly owing to its relatively well-proportioned distribution of Au nanoparticles, which increases the mass transfer among the RGO sheets and Au nanoparticles in the electrode, and ultimately promotes the catalytic properties of electrode. Fig. 5B exhibits the chronoamperograms (CAs) of $Au_{0.25}$/RGO/$Au_{0.75}$/RGO/CF, $Au_{0.5}$/RGO/$Au_{0.5}$/RGO/CF, and $Au_{0.75}$/RGO/$Au_{0.25}$/RGO/CF electrodes in 1.0 M C_2H_5OH/1.0 M KOH solution. It can be seen that the profiles of the curves on these three electrodes are similar to each other, and the current densities on the electrodes during the whole scanning test are closed. The closed current densities in both CVs and CAs indicated that the current densities in the Au/RGO/Au/RGO/CF electrodes do not affected severely by the different distribution of Au nanoparticles among the RGO layers. Hence, in comprehensive view of the above results, the $Au_{0.5}$/RGO/$Au_{0.5}$/RGO/CF electrode is determined to be applied for the ethanol electrooxidation in this work.

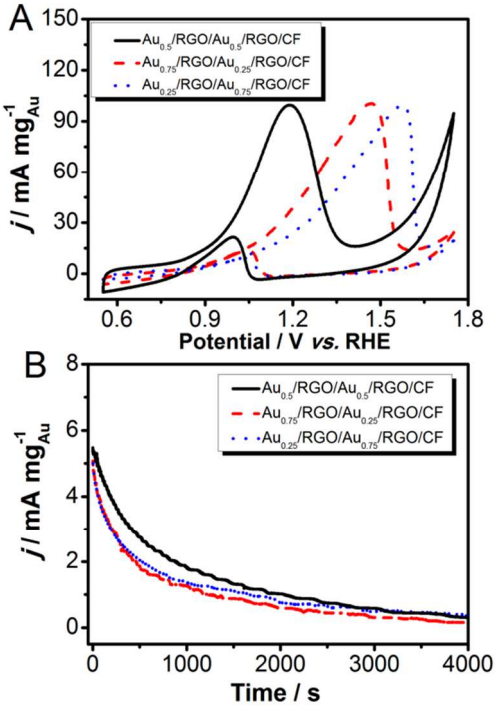

Fig. 5 (A) Cyclic voltammograms (CVs) and (B) chronoamperograms (CAs) of $Au_{0.25}$/RGO/$Au_{0.75}$/RGO/CF, $Au_{0.5}$/RGO/$Au_{0.5}$/RGO/CF, and $Au_{0.75}$/RGO/$Au_{0.25}$/RGO/CF in 1.0 M C_2H_5OH/1.0 M KOH solution, respectively.

As to study the role that the second RGO layer plays in the 3D electrode, ten Au/RGO/CF and RGO/Au/RGO/CF electrodes were prepared, respectively, and four of them were randomly selected to test their electrocatalytic performance. The cyclic voltammograms (CVs) of these electrodes were carried out in 1.0 M C_2H_5OH/1.0 M KOH solution at the same condition, respectively. The peak current densities on each electrode are shown as histogram in Fig. 6. It can be seen that the average of the current densities on RGO/Au/RGO/CF and Au/RGO/CF are closed to each other, which suggests that the catalytic activity of RGO/Au/RGO/CF is near to that of Au/RGO/CF for ethanol electrooxidation. While the current densities on RGO/Au/RGO/CF kept relatively steady compared with that on Au/RGO/CF. According to the results, it can be inferred that the 3D structure of the as-prepared electrode was not closed. And the covered RGO sheets on the surface of electrode act not as an obstructor that blocks the active sites of Au nanoparticles but as frameworks to construct the 3D structure of electrode, so that the reaction species can still cross over the RGO sheets to adsorb and react at the active sites on Au nanoparticles.

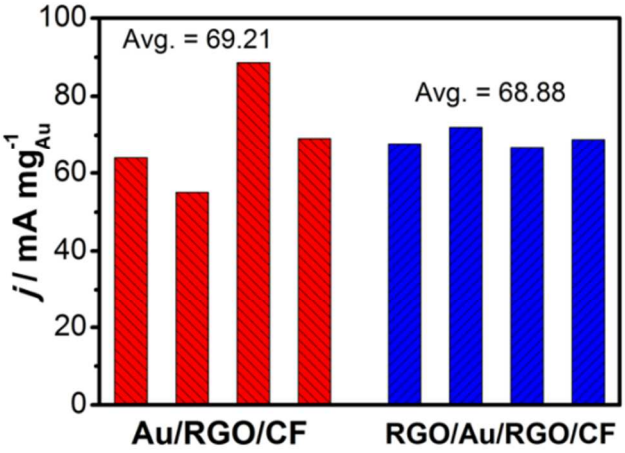

Fig. 6 Histograms of current densities on four different Au/RGO/CF and RGO/Au/RGO/CF electrodes toward ethanol electrooxidation, respectively.

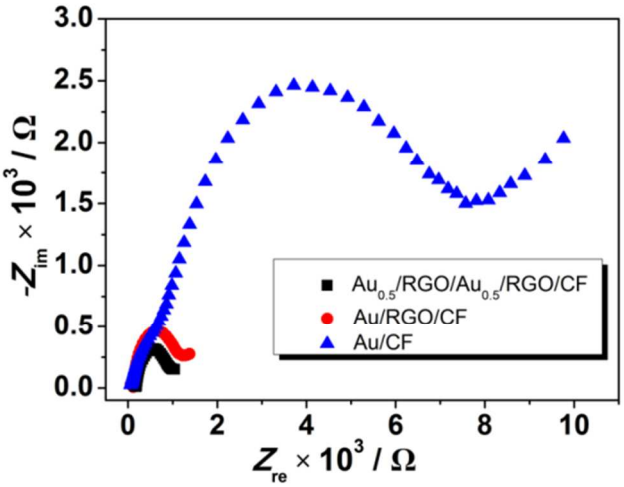

Fig. 7 Nyquist plots of ethanol electrooxidation on $Au_{0.5}$/RGO/$Au_{0.5}$/RGO/CF, Au/RGO/CF and Au/CF electrodes in 1.0 M C_2H_5OH/1.0 M KOH solution at electrode potential of 1.15 V (*vs.* RHE).

Journal of Materials Chemistry A Accepted Manuscript

This journal is © The Royal Society of Chemistry 2012

3.4. The electrochemical impedance spectroscopy study

The electrochemical impedance spectroscopy (EIS) can be used to investigate the interfacial processes and kinetics of electrode reactions and evaluate the electrochemical properties of as-prepared catalysts.[64] EIS on $Au_{0.5}$/RGO/$Au_{0.5}$/RGO/CF, Au/RGO/CF and Au/CF electrodes were investigated at electrode potential of 1.15 V (*vs.* RHE) in 1.0 M C_2H_5OH/1.0 M KOH solution, respectively. The Nyquist plots were recorded in Fig. 7. The impedance arc at high frequencies is generally corresponding to the charge-transfer resistance in the electrode.[65,66] It can be seen from Fig. 7 that the diameter of impedance arc (DIA) on $Au_{0.5}$/RGO/$Au_{0.5}$/RGO/CF, Au/RGO/CF and Au/CF rises in the following order: $Au_{0.5}$/RGO/$Au_{0.5}$/RGO/CF < Au/RGO/CF < Au/CF. The smaller DIAs on $Au_{0.5}$/RGO/$Au_{0.5}$/RGO/CF and Au/RGO/CF suggests that they have better charge transport performance compared with Au/CF electrodes. This is probably attributed to the fact that the RGO sheets with excellent electrical conductivity play vital roles in electron transfer in electrode reaction.[66,67] On the other hand, the particular 3D structure of $Au_{0.5}$/RGO/$Au_{0.5}$/RGO/CF actuates more nanoscale junctions between Au nanoparticles and the RGO sheets, benefiting to the electrons transfer, too.

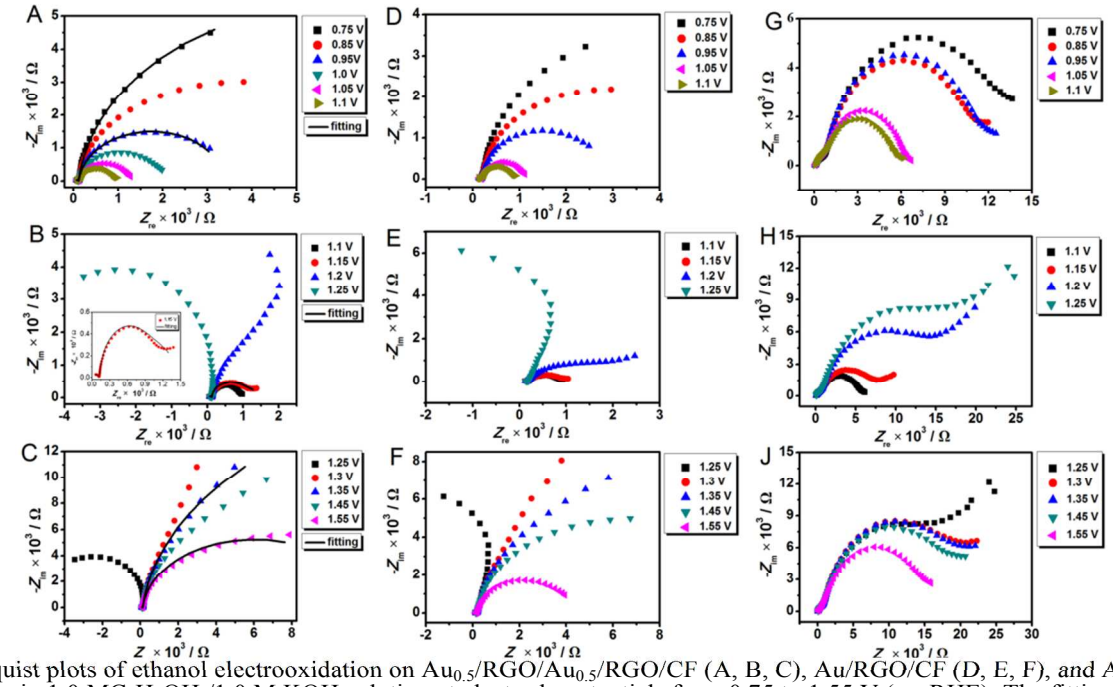

Fig. 8 Nyquist plots of ethanol electrooxidation on $Au_{0.5}$/RGO/$Au_{0.5}$/RGO/CF (A, B, C), Au/RGO/CF (D, E, F), and Au/CF (G, H, J) electrodes in 1.0 M C_2H_5OH /1.0 M KOH solution at electrode potentials from 0.75 to 1.55 V (*vs.* RHE). The fitting lines in (A–C) are representative simulations based on the equivalent circuits in Fig. 9 A and B, respectively.

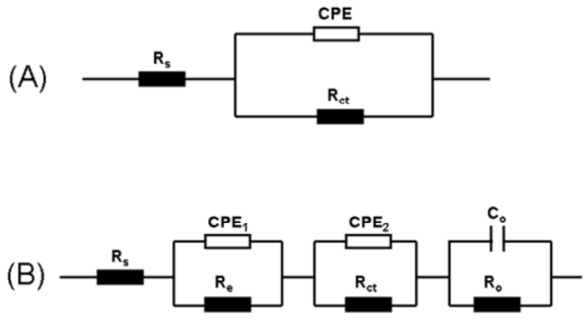

Fig. 9 Equivalent circuits used for simulating the impedance spectra for ethanol electrooxidation on $Au_{0.5}$/RGO/$Au_{0.5}$/RGO/CF at different potentials: (A) at 0.75 to 0.95, and 1.35 ~ 1.55 V (*vs.* RHE); (B) at 1.15 V (*vs.* RHE).

The electron transfer kinetics of ethanol oxidation on $Au_{0.5}$/RGO/$Au_{0.5}$/RGO/CF, Au/RGO/CF and Au/CF were further studied by selected electrochemical impedance spectroscopy (EIS) at various potentials in the range from 0.75 to 1.55 V (*vs.* RHE). Fig. 8 shows the Nyquist plots of ethanol oxidation on $Au_{0.5}$/RGO/$Au_{0.5}$/RGO/CF, Au/RGO/CF and Au/CF in 1.0 M C_2H_5OH/1.0 M KOH solution at different electrode potentials, respectively. Generally, the ethanol oxidation on different electrodes shows different impedance behaviours at different electrode potentials.[65,68-70] For example, for $Au_{0.5}$/RGO/$Au_{0.5}$/RGO/CF (Figs. 8A, B, C), the diameters of the impedance arcs (DIA) in Fig. 8A minished with the increase of the applied potential from 0.75 to 1.1 V. This suggests that the oxidation rate on electrodes is accelerated because of the oxidation removal of intermediates (e.g. alkoxide and acetaldehyde species etc.) that generated during the ethanol dehydrogenation at low potentials occurs, and more and more active sites are available for ethanol oxidation. As the potential continue increasing (Fig. 8B), it can be seen that the DIA starts to increase, which is due to the poisoning and oxidation of Au catalyst at higher potentials. Then the arc begins to reverse obviously at the potential of 1.2 V, and it reverses to the second quadrant at 1.25 V. This is mainly due to the recovery of the catalytic active sites because of the oxidation removal of reaction intermediates by OH_{ads} adsorbed on Au nanoparticles.[62,65] At the potential range between 1.3 V and 1.55 V (Fig. 8C), the arc flips back to the first quadrant with large DIA. This is probably due to that the intermediate species are absent at high potential and the surface of Au is possibly covered by the Au oxides, inhibiting the oxidation of ethanol. As seen from Fig. 8(D, E, F) for Au/RGO/CF, the impedance behaviours is similar to that on $Au_{0.5}$/RGO/$Au_{0.5}$/RGO/CF. However, the arc begins to reverse until the potential is at 1.25 V for Au/RGO/CF. And the DIA of the

Journal of Materials Chemistry A Accepted Manuscript

reversed arc on Au/RGO/CF is larger than that on $Au_{0.5}$/RGO/$Au_{0.5}$/RGO/CF. This implies that the oxidation removal of reaction intermediate species on Au/RGO/CF is slower compared with that on $Au_{0.5}$/RGO/$Au_{0.5}$/RGO/CF. By contrast, the EIS behaviours presented on Au/CF (Fig. 8G, H, J) present many differences with the other electrodes. The arcs on Au/CF in the whole potential range remain in the first quadrant, which indicates the poor activity of oxidation removal of absorbed intermediate species on Au/CF. Herein, the results of the Nyquist plots confirm that the $Au_{0.5}$/RGO/$Au_{0.5}$/RGO/CF possessed highest catalytic activity for ethanol oxidation compared to Au/RGO/CF and Au/CF.

The equivalent circuit is used to fit the EIS data.[65,71,72] On the basis of the above impedance measurements in Fig. 8(A-C), two equivalent circuits for $Au_{0.5}$/RGO/$Au_{0.5}$/RGO/CF are proposed in Fig. 9. Here R_s represents the solution resistance from the relative electrode and the working electrode, R_{ct} is the charge-transfer resistance, and CPE (constant phase element) is the electrode double layer capacitance used instead of a capacitor to account for some complex element in the whole system. In addition, in Fig. 9B, CPE_1 and resistor (R_e) are added in series to fit the high frequency impedance data, which are attributed to a charge-transfer process at the outermost surface of the electrode. And C_o and R_o represent the capacitance and resistance of composite materials on the surface of electrode during the oxidation of adsorbed intermediates species, respectively. Some representative fittings for the $Au_{0.5}$/RGO/$Au_{0.5}$/RGO/CF electrode are shown as solid lines in Fig. 8(A-C), which show good agreement with the corresponding experimental data.

On the basis of the above results and analysis of all the measurements, the enhanced catalytic performances toward ethanol oxidation on $Au_{0.5}$/RGO/$Au_{0.5}$/RGO/CF in alkaline media can be explained as the following reasons. Firstly, it should be attributed to the extraordinarily excellent catalytic activity of Au in alkaline media.[13,19] Although Au is traditionally considered to be chemically inert, recent studies show that Au nanoparticles exhibit high catalytic activity. Even, it can surpass platinum in terms of total oxidation current. Meanwhile, Au as catalyst can efficiently perform electron transfer but interacts weakly with reactants and intermediates, and it has low propensity to form surface oxides, so that it does not get poisoned readily.[19] Secondly, the RGO sheets play important roles in the improvement of the catalytic activity of the electrode. The RGO sheets with particular properties (such as large surface area, excellent electron conductivity, etc.) benefit to the electron transfer, and the remaining oxygen-containing groups of RGO are helpful for the oxidation removal of intermediate species during the ethanol oxidation, which were confirmed by the electrochemical impedance spectroscopy study. Thirdly, the interaction between RGO sheets and AuNPs has been confirmed by the XPS analysis, which can enhance the catalytic activity of the electrode. Fourthly and indispensably, due to the particular 3D structure of $Au_{0.5}$/RGO/$Au_{0.5}$/RGO/CF electrode, the layer-by-layer distribution of Au nanoparticles on $Au_{0.5}$/RGO/$Au_{0.5}$/RGO/CF electrode enables the Au particles to disperse more uniform with smaller particle size and to expose more active sites. What's more, there are more interaction states, transmission channels and nanoscale junctions between the Au nanoparticles and RGO sheets as compared with Au/RGO/CF and Au/CF, which is desirable in electrocatalytic reaction. Because of the effects of the above multiple factors, the $Au_{0.5}$/RGO/$Au_{0.5}$/RGO/CF electrode exhibits the highest activity compared with the other two electrodes.

4. Conclusions

The questions presented in the last of introduction section can be answered as the conclusions. The $Au_{0.5}$/RGO/$Au_{0.5}$/RGO/CF electrode with 3D structure was successfully fabricated by the simple layer-by-layer method. The role of graphene in the 3D electrode is important, which acts as frameworks to construct the 3D structure of electrode. And the electrocatalytic activity of RGO/Au/RGO/CF is not inhibited by the covered RGO sheets on the surface of electrode. It is found that synergistic effects between Au nanoparticles and grapheme exist and benefit to improve their catalytic activity. The 3D structure of $Au_{0.5}$/RGO/$Au_{0.5}$/RGO/CF electrode enhances the catalytic activity towards ethanol oxidation. In summary, these multiple factors contribute to the enhanced catalytic performances observed on the 3D $Au_{0.5}$/RGO/$Au_{0.5}$/RGO/CF electrode.

Acknowledgements

This work was supported by the National Natural Science Foundation of China (Grant Nos. 51373111, 51073114, 20933007), the Project of Scientific and Technologic Infrastructure of Suzhou (SZS201207), Suzhou Nano-project (ZXG2012022), the Priority Academic Program Development of Jiangsu Higher Education Institutions (PAPD), and the Academic Award for Young Graduate Scholar of Soochow University, the Opening Project of Xinjiang Key Laboratory of Electronic Information Materials and Devices (XJYS0901–2010–01).

Notes and references

[a] College of Chemistry, Chemical Engineering and Materials Science, Soochow University, Suzhou 215123, P. R. China. Tel.: +86–512–65880089; Fax: +86–512–65880089; E-mail addresses: duyk@suda.edu.cn (Y. Du).

[b] Department Chemistry and Impact Centre, University of Toronto, Toronto M5S 3H6, Canada. E–mail: mingshanzhu@yahoo.com; zhums@iccas.ac.cn.

1 C. Hu, X. Zhai, Y. Zhao, K. Bian, J. Zhang, L. Qu, H. Zhang and H. Luo, *Nanoscale*, 2014, **6**, 2768.

2 A. Santasalo-Aarnio, Y. Kwon, E. Ahlberg, K. Kontturi, T. Kallio and M. T. M. Koper, *Electrochem. Commun.*, 2011, **13**, 466.

3 S. C. S. Lai, S. E. F. Kleijn, F. T. Z. Öztürk, V. C. v. R. Vellinga, J. Koning, P. Rodriguez and M. T. M. Koper, *Catal. Today*, 2010, **154**, 92.

4 D. Chen, Y. Zhao, Y. Fan, X. Peng, X. Wang and J. Tian, *J. Mater. Chem. A*, 2013, **1**, 13227.

5 M. Huang, G. Dong, N. Wang, J. Xu and L. Guan, *Energy Environ. Sci.*, 2011, **4**, 4513.

6 Y. Lu and W. Chen, *J. Phys. Chem. C*, 2010, **114**, 21190.

7 A. Brouzgou, S. Q. Song and P. Tsiakaras, *Appl. Catal., B*, 2012, **127**, 371.

8 Z. Zhang, C. Zhang, J. Sun, T. Kou, Q. Bai, Y. Wang and Y. Ding, *J. Mater. Chem. A*, 2013, **1**, 3620.

9 Z. Bai, P. Xu, S. Chao, H. Yan, Q. Cui, L. Niu, L. Yang and J. Qiao, *Catal. Sci. Technol.*, 2013, **3**, 2843.

10 B. K. Jena and C. R. Raj, *Chem. Eur. J.*, 2006, **12**, 2702.

11 C. R. Raj and B. K. Jena, *Chem. Commun.*, 2005, 2005.

12 M.C. Daniel and D. Astruc, *Chem. Rev.*, 2004, **104,** , 293.

13 P. Rodriguez, Y. Kwon and M. T. M. Koper, *Nature Chemistry*, 2012, **4**, 177.

14 M. Valden, X. Lai and D. W. Goodman, *Science*, 1998, **281** 1647.

Journal of Materials Chemistry A Accepted Manuscript

 This journal is © The Royal Society of Chemistry 2012

15 T. F. Jaramillo, S.-H. Baeck, B. R. Cuenya and E. W. McFarland, *J. Am. Chem. Soc.*, 2003, **125**, 7148.
16 P. Rodriguez, J. M. Feiu and M. T. M. Koper, *Electrochem. Commun.*, 2009, **11**, 1105.
17 J. A. Rodriguez, P. Liu, J. Hrbek, J. Evans and M. Perez, *Angew. Chem. Int. Ed.*, 2007, **46**, 1329.
18 H. Li, Y.J. Li, L.L. Sun and X.L. Zhao, *Electrochim. Acta*, 2013, **108**, 74.
19 P. Rodriguez and M. T. M. Koper, *Phys. Chem. Chem. Phys.*, 2014, **16**, 13583.
20 N. Lopez and J. K. Nørskov, *J. Am. Chem. Soc.*, 2002, **124**, 11262.
21 N. Lopez, *J. Catal.*, 2004, **223**, 232.
22 J. Duan, S. Chen, S. Dai and S. Z. Qiao, *Adv. Funct. Mater.*, 2014, **24**, 2072.
23 M. C. Holz, K. Tölle and M. Muhler, *Catal. Sci. Technol.*, 2014, **4**, 3495.
24 V. I. Sobolev, K. Y. Koltunov, O. A. Simakova, A.R. Leino and D. Y. Murzin, *Appl. Catal., A*, 2012, **433-434**, 88.
25 P. Y. Sheng, G. A. Bowmaker and H. Idriss, *Appl. Catal., A*, 2004, **261**, 171.
26 D. Chen, L. Tang and J. Li, *Chem. Soc. Rev.*, 2010, **39**, 3157.
27 S. Zhang, Y. Shao, H.-g. Liao, J. Liu, I. A. Aksay, G. Yin and Y. Lin, *Chem. Mater.*, 2011, **23**, 1079.
28 Y. Wang, J. Yu, W. Xiao and Q. Li, *J. Mater. Chem. A*, 2014, **2**, 3847.
29 Y. Jiao, Y. Zheng, M. Jaroniec and S. Z. Qiao, *J. Am. Chem. Soc.*, 2014, **136**, 4394.
30 C. Wang, R. Yue, H. Wang, C. Zou, J. Du, F. Jiang, Y. Du, P. Yang and C. Wang, *Int. J. Hydrogen Energy*, 2014, **39**, 5764.
31 F.F. Ren, C.Q. Wang, C.Y. Zhai, F.X. Jiang, R.R. Yue, Y.K. Du, P. Yang and J.K. Xu, *J. Mater. Chem. A*, 2013, **1**, 7255.
32 A. Dutta and J. Ouyang, *Appl. Catal., B*, 2014, **158-159**, 119.
33 R. Devasenathipathy, V. Mani, S.-M. Chen, D. Arulraj and V. S. Vasantha, *Electrochim. Acta*, 2014, **135**, 260.
34 Y. Du, Y. Zhao, Y. Qu, C.-H. Chen, C.-M. Chen, C.-H. Chuang and Y. Zhu, *J. Mater. Chem. C*, 2014, **2**, 4683.
35 P. Wang, Z.G. Liu, X. Chen, F.L. Meng, J.H. Liu and X.J. Huang, *J. Mater. Chem. A*, 2013, **1**, 9189.
36 Z. Yao, M. Zhu, F. Jiang, Y. Du, C. Wang and P. Yang, *J. Mater. Chem.*, 2012, **22**, 13707.
37 L. Ren, K. S. Hui and K. N. Hui, *J. Mater. Chem. A*, 2013, **1**, 5689.
38 X. Chen, Z. Cai, X. Chen and M. Oyama, *J. Mater. Chem. A*, 2014, **2**, 315.
39 T. Y. Ma, S. Dai, M. Jaroniec and S. Z. Qiao, *Angew. Chem. Int. Ed.*, 2014, **53**, 7281.
40 W. S. Hummers, Jr. and R. E. Offeman, *J. Am. Chem. Soc.*, 1958, **80**, 1339.
41 A. Martín and A. Escarpa, *TrAC, Trends Anal. Chem.*, 2014, **56**, 13.
42 S. Bong, Y.-R. Kim, I. Kim, S. Woo, S. Uhm, J. Lee and H. Kim, *Electrochem. Commun.*, 2010, **12**, 129.
43 F. Gao, X. Cai, X. Wang, C. Gao, S. Liu, F. Gao and Q. Wang, *Sens. Actuators, B*, 2013, **186**, 380.
44 A. Khorsand Zak, W. H. A. Majid, M. Ebrahimizadeh Abrishami, R. Yousefi and R. Parvizi, *Solid State Sciences*, 2012, **14**, 488.
45 X. B. Yan, J. T. Chen, J. Yang, Q. J. Xue and P. Miele, *ACS Appl. Mater. Inter.*, 2010, **2**, 2521.
46 P. Santhosh, A. Gopalan and K. Lee, *J. Catal.*, 2006, **238**, 177.
47 A. W. Burton, K. Ong, T. Rea and I. Y. Chan, *Microporous Mesoporous Mater.*, 2009, **117**, 75.
48 P. Ilanchezhiyan, J. J. Eo, A. S. Zakirov, S. D. Gopal Ram, G. N. Panin and T. W. Kang, *Mater. Lett.*, 2014, **124**, 18.
49 R. K. Shervedani and A. Amini, *Electrochim. Acta*, 2014, **121**, 376.
50 D. P. Anderson, R. H. Adnan, J. F. Alvino, O. Shipper, B. Donoeva, J.Y. Ruzicka, H. Al Qahtani, H. H. Harris, B. Cowie, J. B. Aitken, V. B. Golovko, G. F. Metha and G. G. Andersson, *Phys. Chem. Chem. Phys.*, 2013, **15**, 14806.
51 K. Qian, L. Luo, H. Bao, Q. Hua, Z. Jiang and W. Huang, *Catal. Sci. Technol.*, 2013, **3**, 679.
52 Y. Wei, J. Liu, Z. Zhao, A. Duan, G. Jiang, C. Xu, J. Gao, H. He and X. Wang, *Energy Environ. Sci.*, 2011, **4**, 2959.
53 A. N. Geraldes, D. F. da Silva, E. S. Pino, J. C. M. da Silva, R. F. B. de Souza, P. Hammer, E. V. Spinacé, A. O. Neto, M. Linardi and M. C. dos Santos, *Electrochim. Acta*, 2013, **111**, 455.
54 S. Yongprapat, A. Therdthianwong and S. Therdthianwong, *J. Electroanal. Chem.*, 2013, **697**, 46.
55 G. Tremiliosi-Filho, L. H. DaU'Antonia and G. Jerkiewicz, *J. Electroanal. Chem.*, 1997, **422**, 149.
56 F. Yang, K. Cheng, K. Ye, X. Xiao, F. Guo, J. Yin, G. Wang and D. Cao, *Electrochim. Acta*, 2013, **114**, 478.
57 Y. Li, M. van Zijll, S. Chiang and N. Pan, *J. Power Sources*, 2011, **196**, 6003.
58 L. Chen, Y. Tang, K. Wang, C. Liu and S. Luo, *Electrochem. Commun.*, 2011, **13**, 133.
59 X. Han, D. Wang, D. Liu, J. Huang and T. You, *J. Colloid Interface Sci.*, 2012, **367**, 342.
60 R. K. Pandey and V. Lakshminarayanan, *Appl. Catal., B*, 2012, **125**, 271.
61 J. Zhao, M. Shao, D. Yan, S. Zhang, Z. Lu, Z. Li, X. Cao, B. Wang, M. Wei, D. G. Evans and X. Duan, *J. Mater. Chem. A*, 2013, **1**, 5840.
62 J. Yeonyi, *Solid State Ionics*, 2004, **175**, 145.
63 C.-G. Lee, *J. Electroanal. Chem.*, 2013, **701**, 36.
64 D. Xiang and L. Yin, *J. Mater. Chem.*, 2012, **22**, 9584.
65 W. Zhou, Y. Du, F. Ren, C. Wang, J. Xu and P. Yang, *Int. J. Hydrogen Energy*, 2010, **35**, 3270.
66 S. Liu, J. Wang, J. Zeng, J. Ou, Z. Li, X. Liu and S. Yang, *J. Power Sources*, 2010, **195**, 4628.
67 J. B. Xu, T. S. Zhao, Y. S. Li and W. W. Yang, *Int. J. Hydrogen Energy*, 2010, **35**, 9693.
68 R. Yue, F. Jiang, Y. Du, J. Xu and P. Yang, *Electrochim. Acta*, 2012, **77**, 29.
69 E. P. Lee, Z. Peng, W. Chen, S. Chen, H. Yang and Y. Xia, *ACS NANO*, 2008, **2**, 2167.
70 Z.B. Wang, Y.Y. Chu, A.F. Shao, P.J. Zuo and G.P. Yin, *J. Power Sources*, 2009, **190**, 336.
71 A. Chen, D. J. L. Russa and B. Miller, *Langmuir*, 2004, **20**, 9695.
72 G. Wu, L. Li and B.-Q. Xu, *Electrochim. Acta*, 2004, **50**, 1.

Journal of Materials Chemistry A Accepted Manuscript

Graphical Abstract

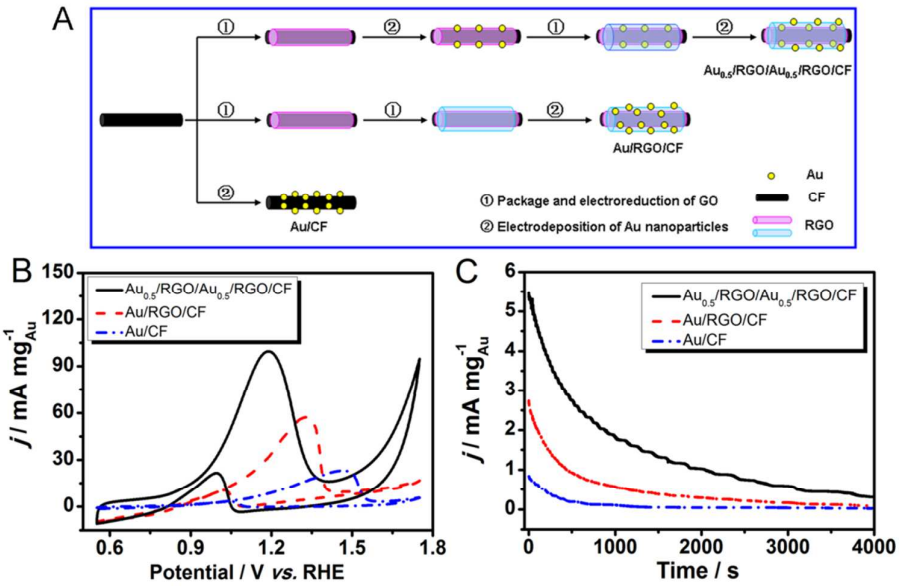

Highly efficient catalytic activity for ethanol electrooxidation on three-dimensional layer-by-layer $Au_{0.5}$/RGO/$Au_{0.5}$/RGO/CF electrode in alkaline medium.

Journal of Materials Chemistry A Accepted Manuscript